

Exciton-polariton bottleneck and the thermalization of polariton luminescence in CdS and CdSe

Farid Askary and Peter Y. Yu*

Department of Physics, University of California, Berkeley, Berkeley, California 94720

(Received 10 September 1984)

The decay in time of polariton luminescence (PL) excited by picosecond laser pulses in CdS and CdSe has been studied both experimentally and theoretically. The time dependence of the PL is measured with a time-resolved photon counting system with subnanosecond resolution. The decays of the PL are found to be approximately single exponentials at low (< 2 K) and high (> 20 K) temperatures. At intermediate temperatures the decays are better approximated by a sum of two exponentials. These experimental results are found to be well reproduced by theoretical calculations based on a two-branch polariton model. Pekar's additional boundary condition is adopted in calculating the time-resolved PL spectra. A comparison between theory and experiment enabled the polariton bottleneck to be identified. Furthermore, it is shown that at finite temperatures the polariton bottleneck enables a quasithermal equilibrium to be established among polaritons.

I. INTRODUCTION

Polaritons result from the coupling of light to polarization modes, such as phonons and excitons, in a medium.¹ In the present paper we are only interested in exciton-polaritons which determine the optical properties of many semiconductors. As a result the term polariton will be understood to mean exciton-polaritons unless otherwise stated.

During the past several decades the properties of polaritons in various semiconductors have been studied extensively by techniques such as transmissivity,² reflectivity,³ photoluminescence,⁴ and resonant light scattering.⁵ As a result of these investigations a large amount of very detailed and precise information has been accumulated about polariton dispersion in semiconductors. However, there are still several outstanding unresolved questions concerning polaritons. One of these is the question of which additional boundary conditions (ABC's), out of the many that have been proposed, is the appropriate one to use in interpreting the experimental results.⁶ Another unresolved question is the quantitative interpretation of polariton emission spectra.⁷ In 1959, based on theoretical arguments, Toyozawa⁸ proposed that the polariton lifetime should reach a maximum at energies close to the transverse exciton energies (this is generally referred to as the polariton bottleneck). So far there has been no conclusive demonstration of this polariton bottleneck⁹ and the role it plays in the relaxation of polariton has not been elucidated.

In the present article we present the results of an experimental and theoretical investigation in the dynamical properties of polaritons in CdS and CdSe, using the time-resolved photoluminescence technique.¹⁰ Although the same technique had been applied by Heim and Wiesner⁹ about ten years ago to CdS, these authors only qualitatively interpreted their results based on the theory of polaritons and they could not identify the polariton bottleneck from their results. By developing a simple two-branch

polariton model from which we can calculate both the time-resolved and steady-state polariton emission spectra, we are able to quantitatively explain our polariton emission spectra and furthermore to demonstrate the role of the polariton bottleneck in the thermalization of polaritons.¹¹ By so doing we have established beyond any reasonable doubt the existence of the polariton bottleneck.

In Sec. II we will present our model calculation of the steady-state and time-resolved polariton emission spectra. In Sec. III we present the experimental setup for obtaining the time-resolved emission spectra in CdS and CdSe and also our experimental results. In Sec. IV we compare these results with the theoretical calculations and with the earlier results of Heim and Wiesner. Finally our discussions and conclusions are presented in Sec. V.

II. THEORY AND MODEL

A. Polariton dispersion

To simplify our calculations, we will make the following assumptions. The semiconductor we are considering has only one electric dipole active exciton band (the 1s state) which is relevant to our calculation. The dispersion of this exciton is isotropic. The energy of the transverse exciton $E_T(k)$ is given by

$$E_T(k) = E_T(0) + \frac{\hbar^2 k^2}{2m^*}, \quad (1)$$

where k is the crystal momentum of the exciton and m^* its effective mass. The dispersion curve of $E_T(k)$ is shown as the dashed curve in Fig. 1. Since the transverse exciton is dipole active, it can couple to electromagnetic waves (photons), whose dispersion is given by

$$\hbar\omega = \frac{ck}{(\epsilon_b)^{1/2}} \quad (2)$$

where c is the speed of light *in vacuo* and ϵ_b is the back-

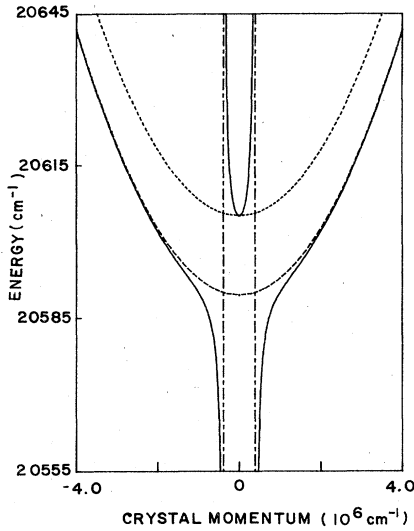


FIG. 1. Dispersion of the A exciton polariton of CdS. Solid curve, polaritons; ---, transverse exciton; ●, longitudinal exciton; -.-.-, photon. Parameters used in this calculation are given in Table I.

ground dielectric constant of the medium excluding the contribution of the exciton. The photon dispersion curve is shown by the dotted-dashed line in Fig. 1. As a result of the coupling of the photons and the transverse excitons, polaritons are formed. It has been shown that under the above assumptions the polariton dispersion can be determined from the implicit equation:⁵

$$\epsilon(k, E) = \frac{\hbar^2 k^2 c^2}{E^2} = \epsilon_b + \frac{4\pi\beta E_T^2(k)}{E_T^2(k) - E^2}, \quad (3)$$

where ϵ is the dielectric function of the medium including the polariton contribution, E is the polariton energy, and β is the polarizability of the exciton. The second term on the right-hand side of Eq. (3) is the contribution of the exciton to the dielectric function. In general, for a given value of k , Eq. (3) has two solutions for E and these are shown as the solid curves in Fig. 1. These two solutions which represent the two propagating modes inside the medium are known as the upper and lower polariton branches. The energy of the dipole inactive longitudinal exciton E_L is given by definition as

$$\epsilon(k, E_L) = 0. \quad (4)$$

From Eq. (3) we obtain therefore the longitudinal exciton dispersion:

$$E_L(k) \simeq E_T(k) + \frac{2\pi\beta}{\epsilon_b} E_T(0). \quad (5)$$

Thus the exciton polarizability β can be determined experimentally from the energy splitting ΔE_{LT} of the longitudinal and transverse exciton at $k=0$. In many previous works a phenomenological damping constant Γ is often introduced in Eq. (3) to account for the finite lifetime of the exciton. We will not adopt this approach here because

we will explicitly include in our model the decay mechanisms which contribute to Γ . This point will be elaborated further when we consider these decay mechanisms.

B. Additional boundary conditions (ABC's) and generalized transmission and reflection coefficients of polaritons

The existence of two polariton branches means that for a given frequency there can exist as many as two propagating waves inside the medium with the same polarization but with different wave vectors. The existence of this additional transmitted wave means that the Maxwell's equations when applied to the fields at the surface of the medium are insufficient for determining uniquely the transmitted and reflected wave amplitudes. Under such circumstances an additional boundary condition (known as an ABC) is needed. Extensive theoretical and experimental investigations of ABC's have already been documented in the literature.¹² However, the situation is far from being clear. Experimental results obtained by different techniques on the same sample seem to require different ABC's.

In connection with this work we have performed reflectivity and steady-state photoluminescence measurements on the same CdS and CdSe samples under identical conditions as the time-resolved emission studies. In interpreting these reflectivity and photoluminescence spectra we have considered these two ABC's. The first one was proposed by Pekar (to be referred to as ABC1) and has the form¹³

$$\left[\sum_i \mathbf{P}_i \right] \Big|_{z=0^+} = 0, \quad (6)$$

where \mathbf{P}_i represents the polarization of the exciton components of the i th polariton branch and the sample is assumed to occupy the half space $Z > 0$. The second ABC we have considered (ABC2) was proposed by Ting *et al.*¹⁴ and can be considered almost the opposite extreme of ABC1:

$$\left[\sum_i \frac{d\mathbf{P}_i}{dz} \right] \Big|_{z=0^+} = 0. \quad (7)$$

If the polariton is regarded as a wave traveling along a string towards the surface, the ABC1 is equivalent to assuming the string is tied down at the surface, while in case of ABC2 the string is completely free at the surface. Many generalized forms of ABC, including ABC1 and ABC2 as limiting cases, have been proposed also.¹⁵ In previous work³ on the reflectivity of CdS it has already been shown that ABC1 with allowance of an exciton-free "dead layer" on the surface can account quite satisfactorily for reflectivity spectra of polaritons in CdS. In a previous paper¹¹ we have shown that ABC1 can also explain the steady-state emission spectra of CdS more satisfactorily than ABC2. As a consequence we will exclusively consider only ABC1 in the present work. We expect that many of the qualitative results we deduce from our model calculation about the polariton relaxation are independent of the ABC chosen.

After the ABC is chosen, it is necessary to consider its

effect on the time-resolved polariton emission curves. The ABC affects the time-resolved emission curves in two respects. Firstly, the ABC affects the transmission and reflection coefficients of the polaritons at the sample surfaces. Since in the experiment only the transmitted polariton energy are detected, this transmission coefficient has to be calculated in order to relate the emission curve to the polariton population. Secondly, the polariton population inside the medium as a function of time is determined by its rate of generation and loss from the medium. The transmission of the polariton out of the medium and conversion of polaritons from one branch to another after reflection at the surface all affect the time evolution of the polariton population and these processes are all dependent on the ABC.

In order to calculate the transmission and reflection coefficients of the polaritons we will introduce the following notation. The amplitude of electric field associated with a polariton mode will be denoted by \mathcal{E}_0 , \mathcal{E}_u , \mathcal{E}_l , or \mathcal{E}_L where the subscripts 0, u , l , and L denote the field in vacuum, the field associated with the upper polariton branch, the lower polariton branch, and the longitudinal branch respectively. A generalized Fresnel coefficient $x_m^{m'}$, where $m, m' = 0, u, l, \text{ or } L$ will be used to denote the field amplitude ratio, is

$$x_m^{m'} = \mathcal{E}_{m'} / \mathcal{E}_m. \quad (8)$$

The subscript m in $x_m^{m'}$ represents the incident field while the superscript m' indicates the reflected or transmitted field. Thus if $m' = m$, $x_m^{m'}$ represents a reflection coefficient while $x_m^{m'}$ ($m' \neq m$) represents a transmission coefficient. From Eq. (3) we can obtain the following simple expression for the Poynting vector for the polaritons and for the longitudinal exciton (details of the derivation are given in the Appendix):

$$\mathbf{S}_u = \frac{c^2}{8\pi\omega} \left[1 - \frac{\chi_u}{\chi_l} \right] |\mathcal{E}_u|^2 \text{Re}(\mathbf{k}_u), \quad (9)$$

$$\mathbf{S}_l = \frac{c^2}{8\pi\omega} \left[1 - \frac{\chi_l}{\chi_u} \right] |\mathcal{E}_l|^2 \text{Re}(\mathbf{k}_l), \quad (10)$$

$$\mathbf{S}_L = \frac{c^2}{8\pi\omega} \left[\frac{16\pi^2 D \omega^2}{\Omega_p^2 c^2} \chi_L^2 \right] |\mathcal{E}_L|^2 \text{Re}(\mathbf{k}_L). \quad (11)$$

\mathbf{k}_u , \mathbf{k}_l , and \mathbf{k}_L denote the wave vector of the upper branch polariton, lower branch polariton, and longitudinal exciton, respectively. The definition of the other quantities can be found in the Appendix. Based on these Poynting vectors, we can define generalized reflection and transmission coefficients $X_m^{m'}$:

$$X_m^{m'} = |\hat{\mathbf{z}} \cdot \mathbf{S}_{m'} / \hat{\mathbf{z}} \cdot \mathbf{S}_m|, \quad (12)$$

where $m, m' = 0, u, l, \text{ or } L$ again. Physically $X_m^{m'}$ represents the fraction of energy normal to the surface of the medium which is transferred from the incident waves (branch m) to the reflected ($m' = m$) or transmitted ($m' \neq m$) wave at the surface. We note that classical relationships such as

$$X_m^m = |x_m^m|^2 \quad (13)$$

are valid only when $m' = m$, but in general $X_m^{m'} \neq |x_m^{m'}|^2$ when $m' \neq m$.

Using ABC1 one can show that for a polariton wave j incident at the surface at angle θ to the normal, energy is conserved for both the s and p polarizations:

$$1 = X_j^0(\theta) + X_j^u(\theta) + X_j^l(\theta), \quad s \text{ polarization} \quad (14)$$

$$1 = X_j^0(\theta) + X_j^u(\theta) + X_j^l(\theta) + X_j^L(\theta), \quad p \text{ polarization}. \quad (15)$$

This is not true for all ABC's and care must be exercised in using the ABC which results in energy being lost or gained at the surface.

C. Rate equation for polariton population

Sumi⁷ was the first to perform a quantitative calculation of the polariton emission curve using a rate equation for the polariton population. However, Sumi neglected the existence of the upper polariton branch and therefore avoided the problem of the ABC. As a result his calculated polariton emission spectra of CdS revealed only the lower energy peak and not the higher energy shoulder or peak as observed in experimental spectra.

In our work we have used Sumi's calculation as the starting point but extended his model to include the upper polariton branch also. As in Sumi's model we assume, for example, that the polariton distribution is spatially homogeneous in a slab of thickness L , is isotropic in momentum space, and is independent of polarization. The latter two assumptions can be justified on the condition that the polaritons are excited well above the bottleneck region so that by the time the polaritons relax down to the region of interest their distributions are already randomized, both in real space and in momentum space, by scattering with phonons. As a result of these assumptions, the polariton distribution function depends only on its energy E . For simplicity we will neglect the longitudinal exciton so that we need to solve only the rate equations for the upper and lower branch polariton populations $\rho_u(E)$ and $\rho_l(E)$:

$$\frac{d\rho_i(E)}{dt} = \left[\frac{d\rho_i(E)}{dt} \right]_{\text{in}} - \left[\frac{d\rho_i(E)}{dt} \right]_{\text{out}}, \quad i = l, u \quad (16)$$

where

$$\left[\frac{d\rho_i(E)}{dt} \right]_{\text{in}}, \quad \left[\frac{d\rho_i(E)}{dt} \right]_{\text{out}}$$

represent, respectively, the rate of generation and the rate of loss of polaritons.

Polaritons with energy E are generated via two possible mechanisms. Polaritons can be excited directly via external radiation fields (with rate S_i) or by scattering in of polaritons from other states (j) via phonons (with rate denoted by $I_{j \rightarrow i}$). The polariton loss rate will be assumed to be the sum of these three dominant processes: (i) radiative loss due to escape of polaritons from the sample surface (P_i), (ii) scattering into other states j due to interaction of acoustic phonons ($Q_{i \rightarrow j}$), and (iii) trapping by impurities (R_i).

For the generation rate S_i we will assume that the excitation source is monochromatic with frequency $\omega_s = E_s / \hbar$

such that E_s lies between E_L and E_L plus one optical phonon energy. For such E_s the upper polariton branch is almost entirely photonlike, while the lower branch is excitonlike so we obtain

$$S_u(E) \propto \delta(E - E_s)$$

and (17)

$$S_l(E) = 0.$$

The polariton-phonon scattering rates $Q_{i \rightarrow j}$ and $I_{j \rightarrow i}$ have been calculated in the same way as reported by Sumi.⁷ Suppose a polariton belonging to branch i with energy E_i , momentum \mathbf{k}_i , and polarization $\hat{\lambda}$ is scattered into another branch j with energy E_j , momentum \mathbf{k}_j , and polarization $\hat{\lambda}$ via scattering with a longitudinal acoustic (LA) phonon of momentum $\mathbf{q} = \mathbf{k}_i - \mathbf{k}_j$ and energy $\hbar\omega = \hbar qu$ (where u is the phonon velocity). The rate for this scattering process can be shown to be given by $W_\lambda(\mathbf{k}_i, \mathbf{k}_j)$ with⁷

$$\begin{aligned} W_\lambda(\mathbf{k}_i, \mathbf{k}_j) = & \frac{2\pi}{\hbar} |V(\mathbf{q})\Phi(E_i, E_j)\sin\theta(\hat{\lambda}, \mathbf{k}_j)|^2 \\ & \times \{ [n(\hbar uq) + 1]\delta(E_i - E_j - \hbar uq) \\ & + n(\hbar uq)\delta(E_i - E_j + \hbar uq) \}, \end{aligned} \quad (18)$$

where $V(\mathbf{q})$ is the matrix element of exciton-acoustic-phonon interaction. Similar to Sumi's approach, we will assume that the exciton interacts with the LA phonon via the deformation potential interaction only. This neglect of the piezoelectric exciton-phonon interaction and of the interaction with the transverse acoustic (TA) phonon greatly simplifies the calculation but, unfortunately, at the same time, it makes the calculation incapable of reproducing detailed features in the polariton population which are necessary for understanding the resonant Brillouin spectra.⁵ However, this approximation has been found to be adequate in reproducing the experimental steady-state polariton luminescence spectra. The definition of the other quantities in Eq. (18) are as follows: n is the occupation number for the acoustic phonon, $\theta(\hat{\lambda}, \mathbf{k}_j)$ is the angle between \mathbf{k}_j and polarization $\hat{\lambda}$, and $\Phi(E_i, E_j)$ is the overlap in the exciton wave functions of polariton branches i and j . $\Phi(E_i, E_j)$ can be expressed in terms of the coefficients C_{ji} introduced by Hopfield.¹⁶ For example for $i=l$ and $j=u$ we have

$$\Phi(E_l, E_u) = [C_{12}(E_l)]^* C_{22}(E_u) + [C_{14}(E_l)]^* C_{24}(E_u), \quad (19)$$

and with the definition of $W_\lambda(\bar{\mathbf{k}}_i, \bar{\mathbf{k}}_j)$ the generation rates $I_{j \rightarrow i}$ and decay rates $Q_{i \rightarrow j}$ can be expressed as

$$I_{j \rightarrow i}(E_i) = \frac{V_c}{(2\pi)^3} \int d^3k_j W_\lambda(\bar{\mathbf{k}}_j, \bar{\mathbf{k}}_i) \rho_j(E_j) \quad (20)$$

and

$$Q_{i \rightarrow j}(E_i) = \frac{V_c}{(2\pi)^3} \int d^3k_j W_\lambda(\bar{\mathbf{k}}_i, \bar{\mathbf{k}}_j) \rho_j(E_j), \quad (21)$$

where V_c is the volume of the crystal.

The polariton trapping rate R_i by defects and impurities is also calculated in the same way as Sumi:⁷

$$R_i(E_i) = R |C_{12}(E)|^2, \quad (22)$$

where R is a parameter assumed to be energy independent and represents the exciton trapping rate.

Finally our calculation of the polariton radiative rate P_i differs from Sumi's⁷ since we have taken into account the existence of the upper branch and the ABC. To calculate P_i we utilized the generalized coefficients X_m^i defined in Eq. (12) and in the Appendix. Since $X_i^i(\omega, \theta)$ represents the fraction of the incident energy contained in polariton branch i , of frequency ω and incident at the surface at angle θ , that is reflected back into the same branch. $1 - X_i^i(\omega, \theta)$ represents the fraction of energy lost (either as a result of transmission or of reflection into the other branches). Thus for a uniform distribution of polaritons belonging to branch i in a slab of thickness L , the radiative loss rate P_i can be expressed as

$$P_i(E_i) = \frac{V_g(E_i)}{2L} \int_0^{\pi/2} \sin\theta \cos\theta [1 - \langle X_i^i(\omega_i, \theta) \rangle_{av}] d\theta, \quad (23)$$

where $\langle X_i^i(\omega_i, \theta) \rangle_{av}$ is the coefficient X_i^i averaged over the s and p polarizations, V_g is the polariton group velocity defined by

$$V_g(E_i) = \frac{1}{\hbar} \frac{dE_i}{dk_i}, \quad (24)$$

and finally the factor of 2 accounts for the fact that only polaritons traveling towards the surface will escape. In our model we have neglected the polaritons that travel into the bulk of the sample.

D. Solutions of the rate equations

For the case of continuous-wave excitation, the polariton rate equation can be solved readily as

$$\rho_i(E) = \frac{S_i(E) + I_{i \leftarrow u}(E) + I_{i \leftarrow l}(E)}{P_i(E) + Q_{i \rightarrow u}(E) + Q_{i \rightarrow l}(E) + R_i(E)}, \quad i=l, u \quad (25)$$

and from the calculated ρ_i the luminescence spectra measured outside the sample can be computed. Results obtained this way for different semiconductors both as a function of temperature and impurity trapping rate have already been presented elsewhere,¹¹ so they will not be repeated here. Instead we will concentrate on the time-dependent solutions to the rate equation.

For the time-dependent solutions we impose the initial boundary conditions that the polaritons are excited at $t=0$ with a monoenergetic distribution, i.e.,

$$\rho(E, t) = \rho_0 \delta(E - E_s) \delta(t). \quad (26)$$

Although these boundary conditions violate the uncertainty principle, this is not significant since we are not interested in solutions of ρ near E_s or very close to $t=0$. Figure 2 shows the results of numerical solutions of

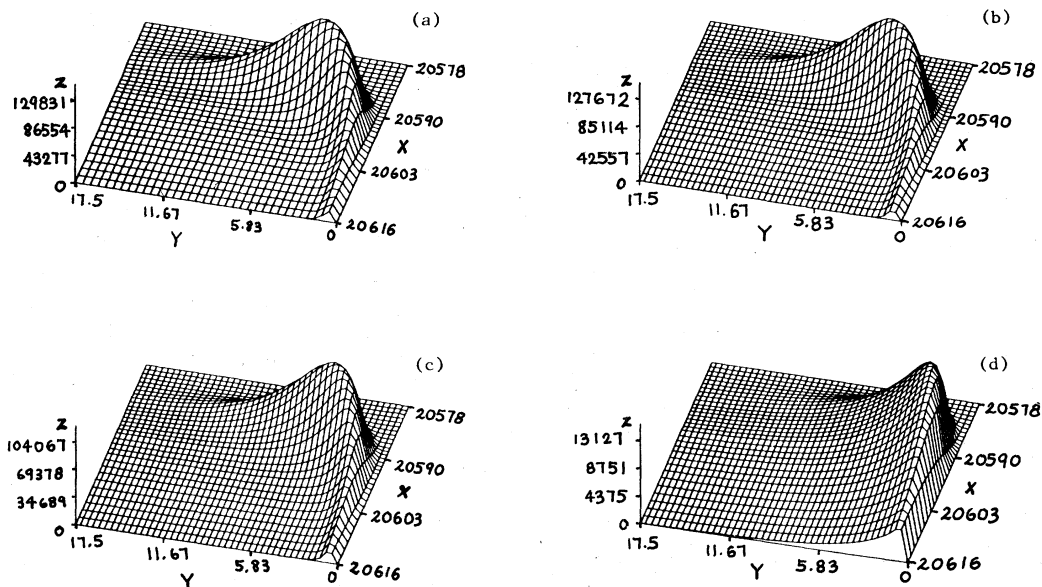


FIG. 2. The lower branch polariton population plotted as functions of time and energy obtained by numerical solution of the rate equation. The coordinate axes are, respectively, as follows: x , energy (cm^{-1}); y , time (nsec); z , population (arbitrary units). The four plots correspond to these four temperatures: (a) 0 K, (b) 1.6 K, (c) 4 K, and (d) 25 K.

$\rho_l(E, t)$ at several different temperatures. The parameters used in the calculation of Fig. 2 are listed in Table I and have been chosen to represent those of the A exciton polariton in CdS. In Fig. 3 the results in Fig. 2 have been replotted on a semilog scale with the peak intensity of all the curves normalized. The purpose of this figure is to show more clearly the time dependence of the lower

branch population for comparison with experiment. In Ref. 11 we have already found that the upper branch population $\rho_u(E, t)$ is insignificant when compared with the lower branch population so the upper branch population is not shown. In Fig. 4 the time dependence of $\rho_l(E, T)$ is plotted on both linear and semilog scales for two different values of impurity trapping rate R at 6 K.

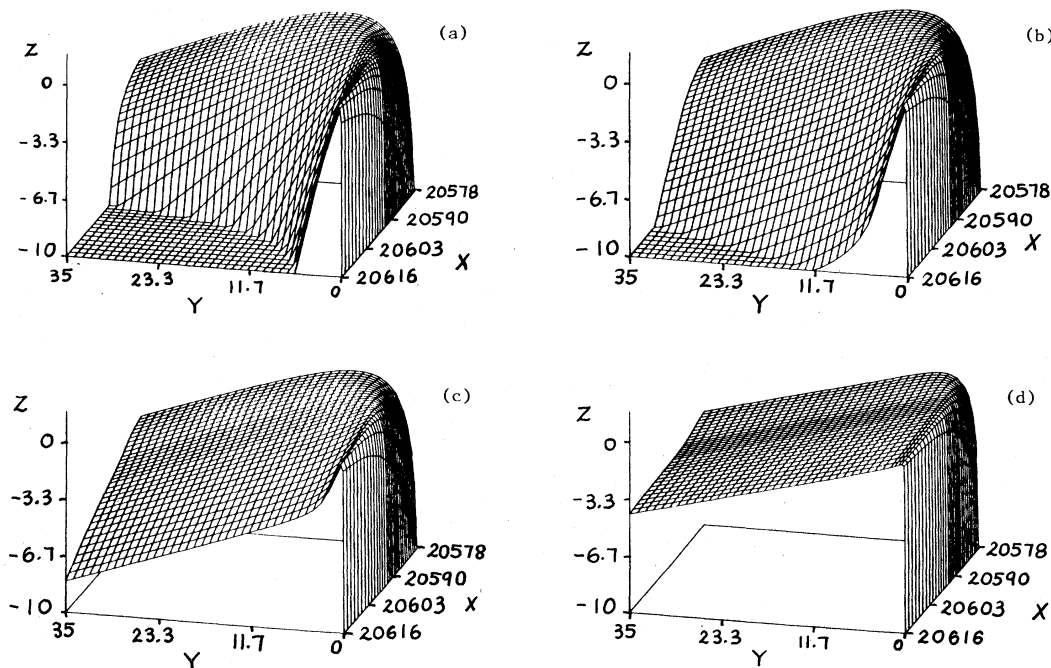


FIG. 3. Same curves as in Fig. 2 except the z axis is now logarithmic and the peaks of all the curves have been normalized.

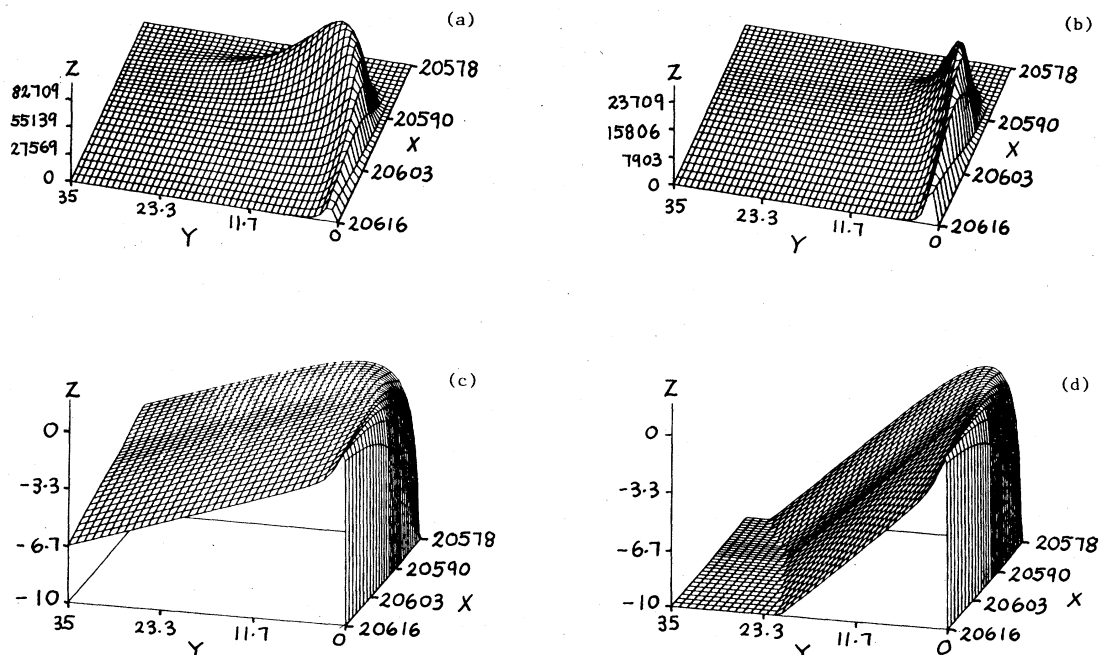


FIG. 4. Plots of polariton population as functions of energy and time showing the effects of impurity trapping rate. The x and y axes are identical to those in Figs. 2 and 3. The z axis in (a) and (b) is linear but logarithmic in (c) and (d). The trapping rate R is equal to $3 \times 10^8 \text{ sec}^{-1}$ in (a) and (b) and equal to $9 \times 10^8 \text{ sec}^{-1}$ in (c) and (d). The sample temperature is assumed to be 6 K.

III. EXPERIMENTAL SETUP AND RESULTS

Time-resolved polariton luminescence (TRPL) spectra of CdS and CdSe samples at liquid-He temperature were obtained with a delayed-coincidence photon-counting system in combination with a mode-locked Ar⁺ or dye laser as the excitation source. Figure 5 is a schematic representation showing the setup. The apparatus is basically similar to the one used by Wiesner and Heim, except our time resolution is better by about a factor of 2. For CdS the 4578-Å line of the mode-locked Ar⁺ laser was used in the excitation source, while for CdSe the output of a synchronously pumped DCM dye laser was used. Details of the

equipment have already been presented elsewhere so will not be elaborated on here.¹⁷

The samples were selected by first examining the PL spectra of several CdS and CdSe samples obtained from various sources. Only samples showing relatively strong PL compared to bound-exciton emission peaks are chosen for TRPL study. In the case of CdS about 4–5 samples satisfy this requirement. However, for CdSe most samples show stronger bound-exciton background. A few samples were found to be inhomogeneous with regard to the strength of the bound-exciton emission peaks. One end of a CdSe sample from the Wright-Patterson Avionic Laboratories was found to have the most prominent PL compared to the bound-exciton emission. Also the location of the bound-exciton and PL peaks in CdSe shows

TABLE I. Parameters used in the calculation of PL spectra of CdS.

Transverse exciton energy (E_T)	20589.5 cm^{-1} ^a
Longitudinal exciton energy (E_L)	20605.0 cm^{-1} ^a
Background dielectric constant (ϵ_b)	9.1 ^b
Exciton effective mass (m^*)	0.94 m_e ^b
Longitudinal acoustic phonon velocity (u)	4.4 $\times 10^5 \text{ cm/sec}$ ^c
Density	4.8 g/cm^3 ^c
Exciton deformation potential	2.5 eV ^c
Thickness of sample (L)	1 μm
Angle of observation outside the crystal (θ)	35°

^aDetermined from experimental reflectivity and steady-state PL spectra.

^bReference 12.

^cReference 7.

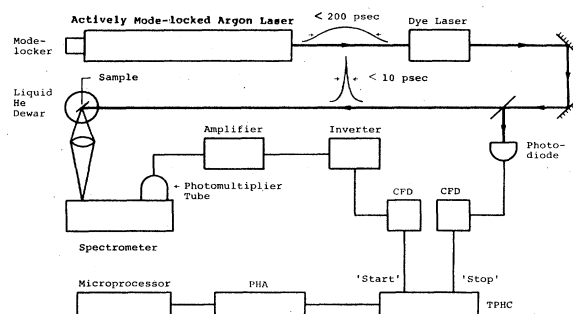


FIG. 5. Schematic representation of the delayed-coincidence photon-counting system. The notations are as follows: CFD, constant fraction discriminator; PHA, pulse-height analyzer; TPHC, time-to-pulse-height converter.

variation from sample to sample in a way that is still not understood.

The measured time-integrated PL spectra in one of our CdS samples and the CdSe sample mentioned above are shown in Figs. 6(a) and 7(a), respectively. A typical TRPL spectra (solid curve) obtained from CdS at ~ 6 K is shown in Fig. 8(a). For comparison the laser pulse measured with the same system is shown as the dashed line. In Fig. 8(b) these two curves have been plotted on a semi-log scale after subtraction of a constant background denoted by B .

To determine the polariton lifetime we have convoluted the laser pulse curve in Fig. 8(b) (regarded as the instrument response curve) with an exponential function of the form $\exp(-t/\tau)$, where the polariton lifetime is adjusted until the convolution curves fits the experimental PL decay curve within noise level. For low temperature ($T \leq 2$ K) the PL decay curves can be fitted satisfactorily by a single exponential decay. However, at higher temperatures, such as $T \sim 6$ K, we found marked discrepancy between the convoluted curve and the experimental curve. This fact was noted also by Wiesner and Heim⁹ but they have nevertheless proceeded to extract a single decay time from the experimental curves. In such cases we have instead convoluted the instrumental response with a sum of two exponentials:

$$f(t) = \sum_{i=1}^2 \alpha_i \exp(-t/\tau_i). \quad (27)$$

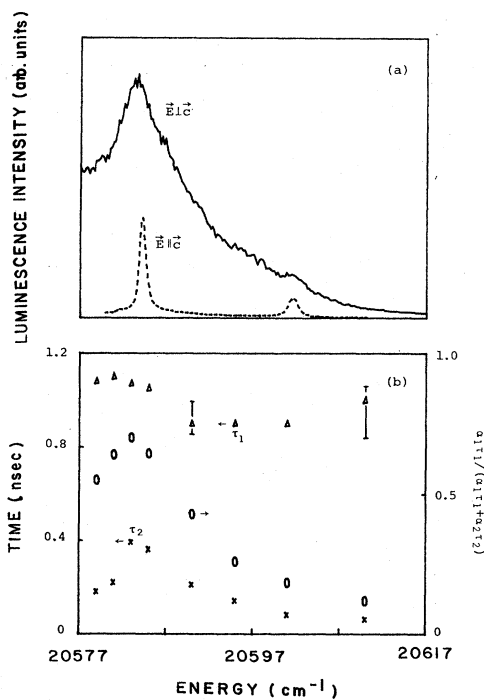


FIG. 6. Summary of the experimental results for CdS at 6 K. (a) Time-integrated luminescence intensity for both E||c and E⊥c. (b) The fast (τ_2) and slow (τ_1) decay times determined from the TRPL spectra as described in the text. The circles represent the fractional amplitude of the slow decay component.

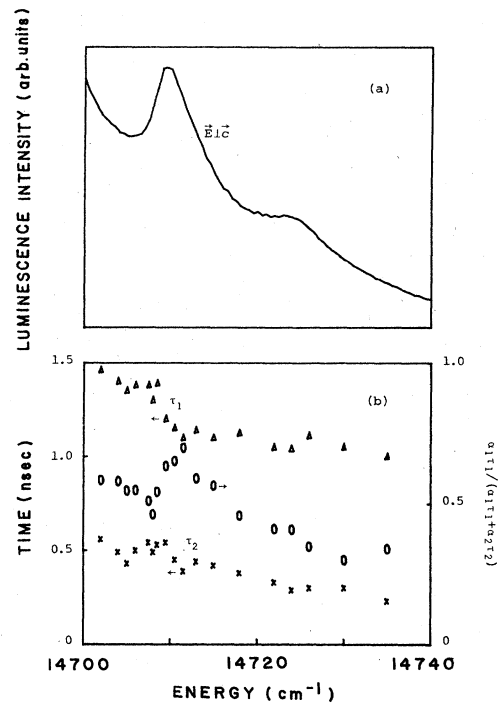


FIG. 7. Summary of the corresponding results in CdSe. Notations are same as in Fig. 6.

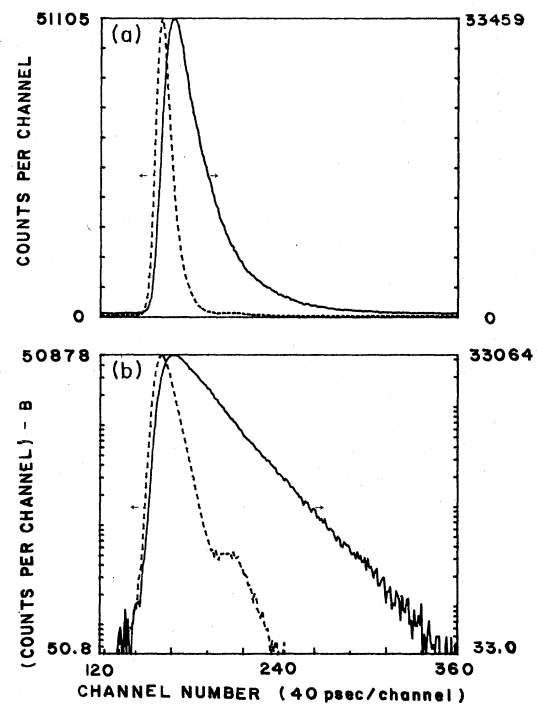


FIG. 8. Typical experimental TRPL spectra plotted on (a) linear scales or in (b) semilog scales after subtraction of a constant background B . The dashed curves in both cases are the instrument response.

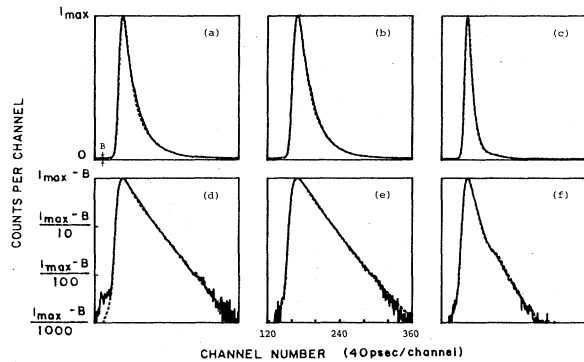


FIG. 9. TRPL spectra of CdS obtained at 6 K for three polariton emission frequencies: (a) and (d), 20 581 cm^{-1} ; (b) and (e), 20 583 cm^{-1} ; (c) and (f), 20 610 cm^{-1} . The dashed curves are fits to the experimental curves (solid curves) by convoluting the instrument response with a sum of two exponential decays. The resultant fast and slow decay times and the fractional amplitude of the slow decay component are displayed in Fig. 6(b).

With a sum of two exponentials we can fit satisfactorily the experimental PL decay curves in all cases. Figure 9 shows some typical two exponential fits (dashed curves) to the experimental spectra (solid curves) for CdS, and Fig. 10 shows the corresponding spectra for CdSe. The decay times τ_1, τ_2 , and the relative weight of the τ_1 (slow) component as measured by $\alpha_1\tau_1/(\alpha_1\tau_1 + \alpha_2\tau_2)$ are shown in Figs. 6(b) and 7(b) for CdS and CdSe, respectively. We have therefore concluded that our results in CdS are basically similar to those observed by Wiesner and Heim with the exception that their CdS sample has a longer polariton lifetime and that we have analyzed our time decays in terms of two exponential decay times.

IV. COMPARISON BETWEEN THEORY AND EXPERIMENT

In this section we will try to interpret both our experimental TRPL results and those of Wiesner and Heim⁹ in

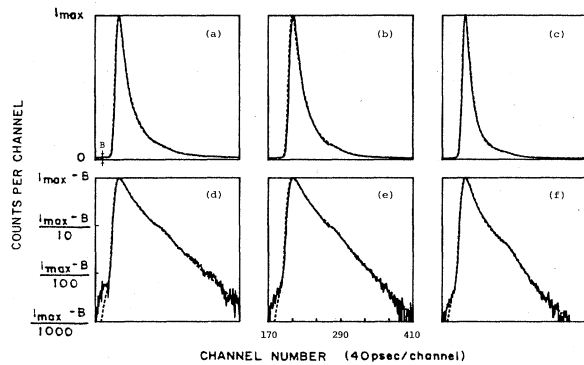


FIG. 10. TRPL spectra of CdSe obtained at 6 K for three polariton emission frequencies: (a) and (d), 14 704 cm^{-1} ; (b) and (e), 14 709.5 cm^{-1} ; (c) and (f), 14 722 cm^{-1} . The corresponding results obtained by analyzing these decay curves with two exponential decays are summarized in Fig. 7(b).

terms of our theoretical results. Since the experimental results are strongly dependent on temperature we will divide them roughly into three temperature ranges as Wiesner and Heim⁹ have also done: (a) low temperature, $T \lesssim 2$ K; (b) intermediate temperatures, $4 \lesssim T \lesssim 15$ K; and (c) high temperatures, $T \gtrsim 20$ K.

At low temperatures Wiesner and Heim⁹ have noted that the PL decays are exponential. Based on Toyozawa's theory,⁸ they expected the decay time to show a maximum which would demonstrate conclusively the existence of the polariton bottleneck. But instead they found that τ reached a plateau and did not decrease below the bottleneck as expected. We found exactly the same behavior in our theory. In Fig. 3(a) we note that the decay of the theoretical TRPL curves is exponential. Furthermore, the slope of the decay ($\propto 1/\tau$) gets progressively less steep as the polariton frequency decreases. However, for polariton frequencies below $\sim 20\,590$ cm^{-1} the decay rate remains more or less constant as observed experimentally. This frequency dependence of τ is shown more clearly in Fig. 11(a). At first these results seem to contradict the Toyozawa theory.⁸ But if we plot the inverse of the total decay rate of the polariton versus frequency [as shown by the solid line in Fig. 11(a)] we find a well-defined maximum as predicted by Toyozawa.⁸ The difference between the two results can be explained by a correct interpretation of the TRPL curves. Suppose polaritons are scattered out of a state at the rate A and created at the rate B . The time dependence of the polari-

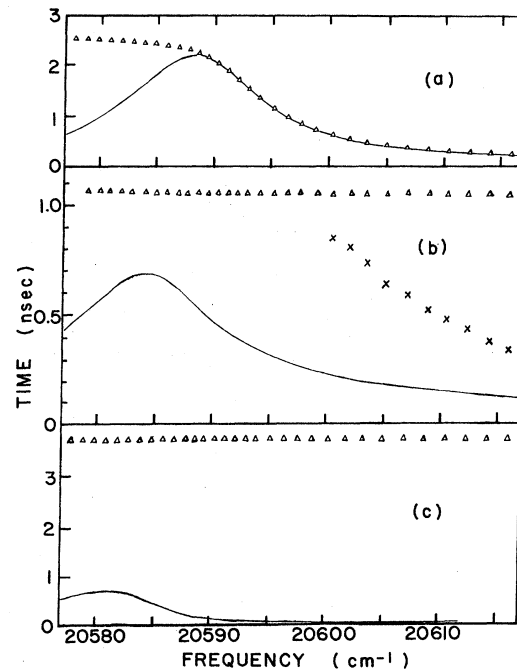


FIG. 11. The slow (triangles) and fast (crosses) decay time constants determined from the theoretical decay curves in Fig. 3 at three different temperatures: (a) 0 K, (b) 6 K (R equal to 8×10^8 sec^{-1} in this case), and (c) 25 K. In all three cases the solid curves represent the reciprocal of the polariton total decay rate.

ton population $\rho(t)$ is then given by

$$\rho(t) \propto \frac{1}{A-B} (e^{-Bt} - e^{-At}). \quad (28)$$

Note that ρ is symmetric with respect to A and B . At long times the decay rate of ρ is dominated by the *smaller* of the two rates. For polaritons above the bottleneck, the decay rates of the polaritons are smaller than the filling rates so the measured decay times are equal to the inverse decay rate as shown in Fig. 11(a). But for polaritons below the bottleneck the opposite is true and the measured decay times are determined by the filling rate. As a result, the decay times of these polaritons are given by the lifetime of the polaritons at the bottleneck. From Fig. 11(a) we locate the polariton bottleneck in CdS at $20\,588\text{ cm}^{-1}$ at 0 K.

At intermediate temperature we found the experimental TRPL decay curves are no longer fitted well by single exponential decays. Instead they are better explained by a sum of two exponential decays. Examination of Figs. 3(b) and 3(c) shows that the theoretical TRPL are also better approximated by two exponential decays. This is particularly evident at $T=4\text{ K}$ [Fig. 3(c)].

In Fig. 11(b) we plot the frequency dependence of the two decay times determined from the theoretical TRPL curves at 6 K. Note that the exciton trapping rate R has been increased in Fig. 11(b) to allow direct comparison with the experimental results in Fig. 6(b). We note that the slow decay time (denoted by τ_1) is approximately frequency independent and is well reproduced by the theoretical result. The fast decay time τ_2 depends on frequency, and this frequency dependence is also reproduced by our theory, although the calculated times are larger approxi-

mately by a factor of 2. By examining the theoretical results we arrive at this interpretation of the two decay times. Initially polaritons are excited by the picosecond laser pulse at energies well above E_T . These polaritons scatter into lower energy states with the fast decay time τ_2 . As these higher energy polaritons relax, they pile up at the bottleneck where the decay rate is smallest. These polaritons in the bottleneck region can scatter back up to higher energy states by absorption of phonons. This "feedback" or up scattering of polaritons from the bottleneck slows the decay of the higher energy polaritons. This explains why the fast decay times τ_2 are different from the inverse decay rates shown in Fig. 11(b) by the solid curve.

If the lifetime of the polaritons at the bottleneck is long compared to the phonon scattering times, a quasithermal equilibrium among polaritons will be attained. When this occurs all the polaritons, independent of energy, will decay with the same lifetime, which is that of the polaritons at the bottleneck. This accounts for the frequency-independent slow decay time τ_1 .

This picture of thermalization among polaritons accounts also for the temperature dependence of the polariton decay. At low temperatures phonon-absorption processes are slow so quasithermal equilibrium is not achieved within the polariton lifetime. At intermediate temperatures these phonon processes are fast compared to the polariton lifetime at the bottleneck so quasithermal equilibrium are achieved typically after $\sim 1\text{ nsec}$. At still higher temperatures quasithermal equilibrium is reached almost instantaneously so the fast decay time τ_2 cannot be measured, and only the frequency-independent decay time τ_1 is observed. This achievement of quasithermal equilibrium by polaritons at 30 K was also noted by Wiesner and Heim.⁹

Finally we observed experimentally essentially the same behavior in CdSe as in CdS, showing that the thermalization procedures described above is applicable to polaritons in general.

V. DISCUSSIONS AND CONCLUSIONS

Once we are convinced of the correctness of our model in explaining the experimental PL results, we can utilize this model to examine other polariton properties. In particular we will use our model to determine the time for the polaritons to reach quasiequilibrium (equilibration time), the effect of impurity trapping on the relaxing process, and the linewidth in Brillouin scattering.

To determine the equilibration time we will plot the PL spectra as a function of time. This is accomplished in Fig. 12 for $T=10\text{ K}$. These spectra show clearly that within the first nanosecond polaritons above the bottleneck at $\sim 20\,588\text{ cm}^{-1}$ builds up due to decay of the higher energy polaritons. In the next 2–3 nsec polaritons start to pile up around the bottleneck at $\sim 20\,588\text{ cm}^{-1}$. About 4–5 nsec after excitation the polariton distribution remains essentially unchanged in shape, indicating that a quasithermal equilibrium has been reached. Beyond $\sim 5\text{ nsec}$ the entire distribution decay with the lifetime of the bottleneck. Thus the equilibration time for the polariton

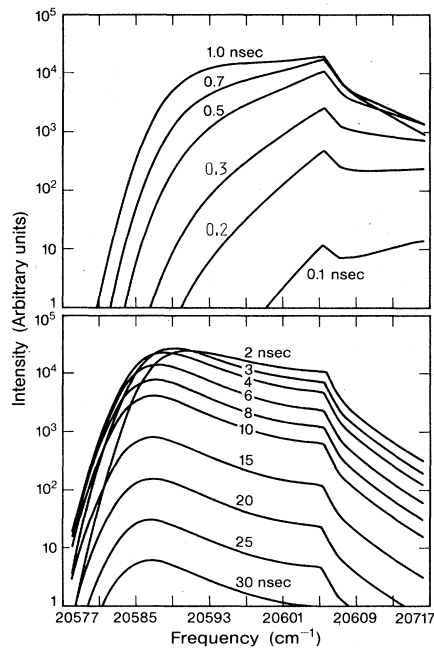


FIG. 12. A series of polariton emission spectra in CdS calculated with the model presented in the text, assuming $T=10\text{ K}$ for various time delays after excitation by a delta-function pulse.

is $\sim 4\text{--}5$ nsec at 10 K, while the lifetime of polaritons at the bottleneck is ~ 2 nsec.

The effect of impurity trapping on the thermalization process can be easily visualized from the PL spectra in Fig. 12. If the polariton lifetime is reduced by trapping to say much less than the equilibration time, the PL spectra will never attain the quasithermal equilibrium line shape. In the nonthermalized line shape there are proportionally larger populations at higher energies. These theoretical spectra can be compared to experimental PL spectra obtained by Travnikov and Krivolapchuk¹⁸ in CdS samples of varying qualities. We note that the PL spectra in Fig. 1 of Ref. 18 are qualitatively reproduced by the theoretical spectra in Fig. 12 at various times. Thus our model provides a quantitative demonstration of the theory proposed in Ref. 18.

In principle our model can be used to calculate the linewidth of Brillouin peaks observed in resonant Brillouin scattering of polaritons.^{6,19} However, we do not expect to find quantitative agreement with experimental results for the following reasons. In our model we have neglected the piezoelectric interaction between excitons and phonons and also the anisotropic exciton dispersion in CdS. The damping of the polariton includes contributions from elastic scatterings. Since these elastic scatterings do not alter the polariton distribution in energy, they have not been included in our calculation. Despite the many simplifying assumptions in our model, we can still use it to estimate the contribution of elastic and inelastic scattering to the Brillouin linewidth in CdS. For $T=0$ K we obtain from Fig. 11(a) a Brillouin linewidth $\gamma=2/\tau$ of ~ 0.05 cm^{-1} at the frequency of 20 605 cm^{-1} . This value is smaller than the experimental value of ~ 0.3 cm^{-1} (Ref. 19) by a factor of 6.

We have found the theoretical fast decay time τ_2 to be larger than our experimental value by a factor of 2, so if we have included also the piezoelectric exciton-phonon interaction we should obtain a Brillouin linewidth of ~ 0.1 cm^{-1} due to inelastic scattering of polaritons. This estimate suggests that the elastic scattering contribution to the experimental Brillouin linewidth is 0.2 cm^{-1} at 20 605 cm^{-1} .

Finally we like to point out the application of our model to interpret other experimental results on polaritons. Using our model we have calculated theoretical reflectivity and transmission spectra in CdS.²⁰ Our results differ little from previous calculations because these spectra are more sensitive to the ABC than to the polariton population. However, in explaining the anomalous wave interference spectra in thin CuCl spectra, Cho²¹ has proposed a phenomenological, frequency-dependent polariton damping of the form

$$\Gamma(E) = \begin{cases} 0.02 \text{ meV}, & E < E_T \\ 0.02 + 0.04(E - E_T)/\Delta E_{LT}, & E > E_T \end{cases} \quad (29)$$

This form of Γ can be easily explained in our model by the phonon scattering rate of the lower branch polaritons.

In conclusion we have developed a two-branch model using the Pekar additional boundary condition. Using this model we have been able to quantitatively or

qualitatively account for these polariton properties in CdS: the steady-state luminescence spectra, the frequency and temperature dependence of the luminescence decay time, the reflection and transmission spectra, and the linewidth of resonant Brillouin scattering. With the help of this model we have demonstrated how polaritons can attain quasithermal equilibrium and have elucidated the role of the polariton bottleneck in the thermalization process.

ACKNOWLEDGMENTS

This project was supported by the National Science Foundation through Grant No. DMR-79-19463. We thank D. C. Reynolds, H. Cummins, and Y. Petroff for generously providing the samples used in the experiment and H. Cummins for sending a report of the resonant Brillouin scattering results in CdS prior to publication.

APPENDIX: POYNTING VECTORS FOR EXCITON POLARITONS

We will obtain expressions for the Poynting vectors associated with the polaritons and the longitudinal exciton using a classical model described by Tait.²² In this model we will assume an isotropic medium with a single dipole resonance. The polarization of the medium \mathbf{P} is decomposed into the sum of a background term \mathbf{P}_b and a term \mathbf{P}_{ex} due to the exciton. The equation of motion neglecting damping for the exciton polarization is written phenomenologically as

$$\ddot{\mathbf{P}}_{ex} + \omega_0^2 \mathbf{P}_{ex} - D \nabla^2 \mathbf{P}_{ex} = -\frac{Ne^2}{m} \mathbf{E}, \quad (A1)$$

where ω_0 is the resonance frequency, N is the density of the dipoles, and the term $D \nabla^2 \mathbf{P}_{ex}$ is introduced to allow for coupling between the dipoles. One can derive the dielectric function of this spatially dispersive medium as

$$\epsilon(k, \omega) = \epsilon_b + \frac{\Omega_p^2/4\pi}{\omega_0^2 + Dk^2 - \omega^2 - i\omega\Gamma}, \quad (A2)$$

where $\Omega_p^2 = 4\pi Ne^2/m$. Equation (A2) is basically the same as Eq. (3) with $D = \omega_0/m$, $\hbar\omega_0 = E_T(0)$, and $4\pi\beta E_T^2(0) = \hbar^2 \Omega_p^2/(4\pi)$ except for the absence of the term proportional to k^4 in Eq. (A2).

Using the Maxwell's equations, one can show that the Poynting theorem is satisfied for this spatially dispersive medium if one defines a Poynting vector by

$$\mathbf{S} = \frac{c}{4\pi} (\mathbf{E} \times \mathbf{H}) + \mathbf{S}_M, \quad (A3)$$

where \mathbf{S}_M is the mechanical part of the energy flow given by

$$\mathbf{S}_M = -\frac{4\pi D}{\Omega_p^2} [\dot{\mathbf{P}} \times (\nabla \times \mathbf{P}) + \dot{\mathbf{P}} (\nabla \cdot \mathbf{P})]. \quad (A4)$$

For transverse plane waves $\mathbf{E}_i(\mathbf{x}, t) = \mathcal{E}_i e^{i(\mathbf{k}_i \cdot \mathbf{x} - \omega t)}$ and

$$\mathbf{H}_i(\mathbf{x}, t) = \frac{c}{\omega} \mathbf{k}_i \times \mathcal{E}_i e^{i(\mathbf{k}_i \cdot \mathbf{x} - \omega t)},$$

where the index $i = u, l$ denotes the upper and lower polariton branches, we obtain the Poynting vectors:

$$\mathbf{S}_u = \frac{c^2}{8\pi\omega} \left[1 - \frac{\chi_u}{\chi_l} \right] |\mathcal{E}_u|^2 \text{Re}(\mathbf{k}_u), \quad (\text{A5})$$

$$\mathbf{S}_l = \frac{c^2}{8\pi\omega} \left[1 - \frac{\chi_l}{\chi_u} \right] |\mathcal{E}_l|^2 \text{Re}(\mathbf{k}_l), \quad (\text{A6})$$

where $4\pi\chi_u = \epsilon(k(E_u), E_u) - \epsilon_b$ and similarly for χ_l .

For the longitudinal exciton where $\epsilon(k(\omega_L), \omega_L) = 0$, there are no magnetic fields and the term involving $\nabla \times \mathbf{P}$

in Eq. (A3) vanishes. The Poynting vector is then given by

$$\mathbf{S}_L = \frac{c^2}{8\pi\omega} \left[\frac{(4\pi)^2 D \omega^2}{\Omega_p^2 c^2} \chi_L^2 |\mathcal{E}_L|^2 \right] \text{Re}(\mathbf{k}_L) \quad (\text{A7})$$

where $4\pi\chi_L = \epsilon(k(E_L), E_L) - \epsilon_b = -\epsilon_b$. Expression (A7) provides the energy flow rate for the longitudinal component which is entirely mechanical (since it is proportional to D) as expected.

*To whom correspondence should be addressed.

¹See, for example, a series of review articles by D. L. Mills and E. Burstein, *Comments Solid State Phys.* **1**, 202 (1969).

²See, for example, W. C. Tait and R. L. Weiher, *Phys. Rev.* **166**, 769 (1968); D. D. Sell, *Phys. Rev. B* **6**, 3750 (1972).

³See, for example, J. J. Hopfield and D. G. Thomas, *Phys. Rev.* **132**, 563 (1963); D. D. Well, S. E. Stokowski, R. Dingle, and J. V. DiLorenzo, *Phys. Rev. B* **10**, 4568 (1973); F. Evangelisti, A. Frova, and F. Patella, *ibid.* **10**, 4253 (1974).

⁴See, for example, E. Gross, S. Permogorov, V. Travnikov, and A. Selkin, *Solid State Commun.* **10**, 1071 (1972); S. Suga, K. Cho, and P. Heisinger, *J. Lumin.* **12/13**, 109 (1976).

⁵See, for example, P. Y. Yu, in *Excitons*, Vol. 14 of *Topics in Current Physics*, edited by K. Cho (Springer, New York, 1979); C. Weisbuch and R. Ulbrich, in *Light Scattering in Solids III*, Vol. 57 of *Topics in Applied Physics*, edited by M. Cardona and G. Güntherodt (Springer, New York, 1982).

⁶See, for example, recent work by J. Wicksted, M. Matsushita, H. Z. Cummins, T. Shigenari, and X. Z. Lu, *Phys. Rev. B* **29**, 3350 (1984).

⁷H. Sumi, *J. Phys. Soc. Jpn.* **41**, 526 (1976).

⁸Y. Toyozawa, *Prog. Theor. Phys. Suppl.* **12**, 111 (1959).

⁹U. Heim and P. Wiesner, *Phys. Rev. Lett.* **30**, 1205 (1973); P. Wiesner and U. Heim, *Phys. Rev. B* **11**, 3071 (1975).

¹⁰A brief publication of our work has already appeared in *Phys. Rev. B* **28**, 6165 (1983).

¹¹Comparison of our theoretical results with steady-state polariton emission spectra has already been presented in F. Askary and P. Y. Yu, *Solid State Commun.* **47**, 241 (1983).

¹²See P. Y. Yu and F. Evangelisti, *Phys. Rev. Lett.* **42**, 1642 (1979) and references therein.

¹³S. I. Pekar, *Zh. Eksp. Teor. Fiz.* **33**, 1022 (1957); **34**, 1176 (1958) [*Sov. Phys.—JETP* **6**, 785 (1958); **7**, 813 (1958)].

¹⁴C. S. Ting, M. J. Frankel, and J. L. Birman, *Solid State Commun.* **17**, 1285 (1975).

¹⁵J. J. Hopfield and D. G. Thomas, *Phys. Rev.* **132**, 563 (1963).

¹⁶J. J. Hopfield, *Phys. Rev.* **112**, 1555 (1958).

¹⁷J. S. Weiner and P. Y. Yu, *J. Appl. Phys.* **55**, 3889 (1984).

¹⁸V. V. Travnikov and V. V. Krivolapchuk, *Pis'ma Zh. Eksp. Teor. Fiz.* **36**, 196 (1982) [*JETP Lett.* **36**, 242 (1982)].

¹⁹T. Shigenari, X. Z. Lu, and H. Z. Cummins, *Phys. Rev. B* **30**, 1962 (1984).

²⁰Farid Askary, Ph.D. thesis, University of California, Berkeley, California, 1983 (unpublished).

²¹Quoted by T. Mita and N. Nagasawa, *Solid State Commun.* **44**, 1003 (1982).

²²W. C. Tait, *Phys. Rev.* **5**, 648 (1972).